Scientific Research Publishing

Open Journal of Fluid Dynamics, 2025, 15(2), 87-115
https://www.scirp.org/journal/ojfd
ISSN Online: 2165-3860
ISSN Print: 2165-3852

Analysis of Heat and Mass Transfer in MHD Free Convection with Chemical Reaction Effects on a Moving Vertical Porous Plate

Toha François Lihonou[1,2*], Abdelghani Laouer[3], Kalil Pierre Mathos[1], Faya Maurice Yombouno[1]

[1]Department of Physics, Faculty of Sciences and Techniques, University of N'Zérékoré, Republic of Guinea
[2]LMFDNMSB Laboratory, IMSP/UAC, Porto-Novo, Benin
[3]LPMCN Laboratory, Faculty of ESCS, University of Jijel, Jijel, Algeria
Email: *lihonoutof@gmail.com

How to cite this paper: Lihonou, T.F., Laouer, A., Mathos, K.P. and Yombouno, F.M. (2025) Analysis of Heat and Mass Transfer in MHD Free Convection with Chemical Reaction Effects on a Moving Vertical Porous Plate. *Open Journal of Fluid Dynamics*, **15**, 87-115.
https://doi.org/10.4236/ojfd.2025.152006

Received: April 10, 2025
Accepted: June 3, 2025
Published: June 6, 2025

Abstract

This study focuses on the numerical investigation of fluid flow, heat transfer, and free MHD convection through a semi-infinite vertical porous plate, considering the effects of chemical reactions. By analyzing the boundary layer, a flow model was developed to represent the governing equations for movement, energy, and concentration, which are time-independent. These equations are expressed as a dimensionless nonlinear system and mathematically transformed into nonlinear ordinary differential equations (ODEs). The ODEs of the model are solved using the BVP4C method within the Matlab R2024B package. Numerical calculations were performed, and the results were analyzed to explore the effects of various parameters such as the magnetic parameter, the permeability of the porous medium, the Eckert number, the Grashof number, the modified Grashof number, the Schmidt number, the heat source parameter, the Prandlt number, the Dufour number, the blowing/suction velocity, the chemical reaction parameter and the Soret number on the velocity, temperature, and concentration profiles, as well as the skin friction coefficient, Nusselt number, and Sherwood number. The study reveals that an increase in magnetic parameters reduces the velocity profiles and increases the temperature and concentration profiles. An increase in the chemical reaction rate decreases the velocity and concentration distributions but increases the temperature profile. Higher injection velocities enhance the profiles, while suction reduces them.

Keywords

MHD Free Convection, Moving Vertical Plate, BVP4C Technical, Injection/Suction

1. Introduction

Heat transfer is a fundamental phenomenon in many scientific fields. In fluids, it refers to the transfer of thermal energy from one location to another. Free convection is a mode of heat transfer in which fluid motion is driven by buoyancy forces rather than by an external source. It is associated with natural convection processes and involves factors such as heat transfer coefficients and thermodynamic laws. Hossain *et al.* [1] investigated MHD free convection and mass transfer flow through a vertically oscillating porous plate in the presence of Hall and ion slip currents, a heat source, and a rotating system. The results of this investigation are discussed for the different values of the well-known parameters and are shown graphically. The effects of a heat source and stratification phenomena on the magnetohydrodynamic (MHD) Prandtl model were studied by Khan *et al.* [2]. They demonstrated that an increase in the stratification parameter leads to a reduction in temperature. S. Zeb *et al.* [3] examined the stagnation point flow of a Prandtl fluid along a stretched sheet in a permeable medium, integrating natural convection, magnetic field effects, heat generation, thermal radiation, and Soret and Dufour phenomena. The main results reveal that porosity significantly increases the wall friction coefficient, while increasing the heat source parameters reduces the Nusselt number. In addition, chemical reaction parameters significantly increase the concentration distribution. The flow and heat transport in an Eyring-Powell fluid under the influence of mixed convection over a graded surface were studied by Bilal and Ashbar [4]. It was found that the velocity and temperature profiles decrease with enhanced thermal stratification, while both increase with the heat generation parameter. The fusion energy phenomena in the Prandtl MHD fluid through an inclined stretched cylinder were solved numerically by Awais *et al.* [5]. They showed that the temperature increases with an increase in the fusion parameter while it decreases with an increase in the magnetic parameter. The analysis of mass and heat transport in the Prandtl-Eyring fluid in oscillatory flow along a permeable channel was discussed by Khafajy and Kaabi [6]. The results show that the velocity of both types of flow, Poiseuille and Couette, increases as the parameters Reynolds, Darcy, Grashof number, radiation parameter, and static pressure rise. The heat and mass transport of Casson fluid along a cylinder in a permeable medium with Soret-Dufour, stagnation point, and suction/injection effects were studied by Alizadeh *et al.* [7]. Ibrahim and Hindebu [8] analyzed MHD boundary layer flow of Eyring-Powell nanofluids using the Cattaneo-Christov heat-mass fluxes theories. The flow model equations, induced by a stretching cylinder, were solved numerically using the Keller-Box technique. They reported that the Nusselt number increased with the Prandtl number, curvature parameter, thermal relaxation time, and the Eyring-Powell fluid parameter. Meanwhile, Layek *et al.* [9] investigated the combined transport of heat and mass transfer for unsteady, incompressible, viscous Eyring-Powell fluid along expanding/shrinking sheets with suction/injection, Dufour and Soret effects. According to their results, the fluid velocity is high for the Eyring-Powell fluid, but Prandtl number and thermal

radiation lessen the fluid temperature. Moreover, an analysis of nonlinear stratified convection of Eyring-Powell fluid past a sheet, which is inclined and stretching with Cattaneo-Christov heat-mass flux model is presented by Jabeen *et al.* [10]. Their analysis revealed that the thermal stratification parameter and Cattaneo-Chiristov time relaxation dampen the distribution of fluid temperature. Salah [11] examined the flow and heat transfer of dissipative and chemically reacting MHD Eyring-Powell fluid past an exponentially stretching sheet under a non-Fourier heat conduction model. The study revealed that both the thermal relaxation time and the Eyring-Powell fluid parameter are inversely related to the temperature profile, while the Eckert number has a positive effect on the temperature profile. Naseem *et al.* [12] analyzed the convection of MHD Eyring-Powell fluid over an exponentially stretching sheet. Their study incorporated the Cattaneo-Christov heat flux model and concluded that both the temperature field and the thermal boundary layer thickness decrease with an increase in the thermal relaxation time parameter, but increase with the Eckert number. It was also observed that the velocity of the Eyring-Powell fluid is higher than that of a Newtonian (viscous) fluid, whereas the opposite is true for the fluid temperature. Furthermore, the magnetic field exhibited a retarding effect on the velocity field while enhancing the temperature distribution. In the last decade, the study of chemical reactions has been a process that leads to the transformation of one set of chemical substances into another. Conventionally, chemical reactions encompass changes that only involve electron positions in the formation and breaking of chemical bonds between atoms without modification of the nuclei. Nuclear chemistry is a subdiscipline of chemistry that involves the chemical reactions of unstable and radioactive elements where both electronic and nuclear changes can occur. Chemical reactions occur at a characteristic reaction rate at a given temperature and chemical concentration. Heat is always generated during these chemical reactions. Most common fluids, such as water and air, are contaminated with impurities such as CO_2, C_6H_6, and HCl, etc. The chemical reaction parameter exhibits a retarding effect on the concentration distribution as the reaction transitions from a constructive to a destructive state. The heat transfer of the radiated Casson fluid in a stagnation point flow with a magnetic field and a chemical reaction was explored by Anwar *et al.* [13]. The study highlights the mutually reinforcing impacts of thermal radiations and chemical processes on the heat transfer process. Jalili *et al.* [14] examined the nonlinear radiative heat transport of Casson fluid flow along a vertical plate with a porous medium, chemical reaction, Joul heating, viscous dissipation, and stratification phenomena. Their analysis showed that increasing the Casson fluid parameter enhances the fluid's velocity field while reducing its concentration and temperature profiles. Khan *et al.* [15] studied the sliding flow and heat transport of a tangent hyperbolic fluid along a rotating greasy sheet. They revealed that the temperature profile and Nusselt number exhibit increasing behavior as the radiation parameter increases. The effect of heat generation on boundary layer fluid flow is very significant due to technical applications such as fire and combustion,

metal scrap, radioactive materials, reactor safety analysis, spent nuclear fuel, etc. Convective heat transfer is generally classified into two basic types. When no externally induced flow is present and the fluid motion arises solely due to density differences caused by temperature or concentration gradients within a body force field, such as gravity, the process is known as natural convection. On the other hand, if the fluid movement is caused by an external agent, such as the externally imposed flow of a fluid stream over a heated object, the process is called forced convection. In forced convection, the fluid flow is generated by an external source such as a fan, a blower, and wind or the movement of the heated object itself. Such problems are frequently encountered in technological applications, where heat transfer to or from a body often occurs due to an externally imposed flow of fluid at a temperature different from that of the body. In contrast, in natural convection, fluid motion is driven by buoyancy forces that arise from density differences caused by temperature or concentration variations. A heated body that cools in the ambient air generates such a flow in the region around it. Similarly, buoyant flow results from the rejection of heat to the atmosphere and other ambient media, circulations occurring in heated rooms, in the atmosphere and in bodies of water, the rise of buoyant flow causing thermal stratification of the medium, as in temperature inversion and many other heat transfer processes in our natural environment, as well as in many technological applications, are included in the field of natural convection. Flow can also occur due to concentration differences, such as those caused by salinity differences in the sea and composition differences in the chemical treatment unit, and these cause mass transfer by natural convection. The effects of radiation and chemical reaction on unsteady MHD heat and mass transfer of Casson fluid flow past a vertical plate were discussed by Biswas *et al.* [16]. Finally, they obtained that velocity decreases with an increase in Casson parameter, Permeability of porous medium and Chemical reaction while it increases with increasing values of Radiation parameter and Grashof number. Temperature increases due to Radiation parameter but decreases for Prandtl number. The effects on the magnetic field during compressional flow of a Casson fluid between parallel plates were explored by Ahmed *et al.* [17]. In their study, it is observed that magnetic field can be used as a control phenomenon in many flows as it normalizes the flow behavior. The influence of the induced magnetic field on the incompressible Prandtl fluid across a stretched plate with homogeneous and heterogeneous reactions was studied by Meenakumari *et al.* [18]. The authors observed that the large values of the stretching ratio and the induced magnetic parameters are primarily moderate magnetic field, velocity, and temperature. Also, the authors found more velocity and temperatures by boosting the slip parameters. The effect of thermodiffusion, Soret and heat generation effects, radiation and chemical reaction effects on MHD, etc., has been presented by Kataria and Patel [19]-[21]. The effect of the magnetic field through the analysis of the linear temporal stability of the flow of a viscous, incompressible and electrically conductive fluid forming a dynamic laminar boundary layer on an impermeable horizontal flat magnetic plate

is presented by Lihonou *et al.* [22].

The aim of this paper is to study and analyze the effects of various parameters, such as the magnetic parameter, permeability of the porous medium, Eckert number, Prandtl number, Soret number, Schmidt number, heat source parameter, chemical reaction parameter, Grashof number, modified Grashof number, Dufour number, and injection/suction velocity-on particle velocity, temperature and concentration profiles, as well as on the skin friction coefficient, Nusselt number, and Sherwood number for a steady MHD heat and mass transfer flow through a vertical porous plate. To achieve this objective, the paper is organized as follows: Section 2 presents the mathematical formulation of the problem; Section 3 describes the numerical solution method; Section 4 discusses and analyzes the results; and the conclusion is provided in the final section.

2. Mathematical Modeling

2.1. Governing Equations

The continuity, momentum, energy and concentration equations for a viscous, incompressible and electrically conductive fluid are given by:

$$\nabla \cdot V = 0, \tag{1}$$

$$\frac{\partial V}{\partial t} + (V \cdot \nabla)V = -\frac{1}{\rho}\nabla p + \nu\nabla^2 V + \frac{1}{\rho}J \wedge B - \frac{\nu}{k^*}V + g\beta_T (T - T_\infty) + g\beta_c (C - C_\infty), \tag{2}$$

$$\frac{\partial T}{\partial t} + (V \cdot \nabla)T = \frac{k}{\rho C_p}\nabla^2 T + \frac{Q}{\rho C_p}(T - T_\infty) + \frac{D_m k_T}{C_s C_p}\nabla^2 C + \frac{\mu}{\rho C_p}(\nabla V)^2, \tag{3}$$

$$\frac{\partial C}{\partial t} + (V \cdot \nabla)C = D_m \nabla^2 C - k_1 (C - C_\infty) + \frac{D_m k_T}{T_m}\nabla^2 T, \tag{4}$$

$$\nabla \wedge B = \mu_e (J + \varepsilon_e E), \tag{5}$$

$$\nabla \wedge E = -\frac{\partial B}{\partial t}, \tag{6}$$

$$\nabla \cdot B = 0, \tag{7}$$

$$\nabla \cdot E = 0, \tag{8}$$

$$\nabla \cdot J = 0, \tag{9}$$

where Equations (1)-(9) are continuity, Newton's second law, energy, concentration, Ampere's law, Faraday's law, Maxwell's law and Gauss law equations respectively, with

$$J = \sigma (E + V \wedge B), \tag{10}$$

Here $V(u, v, w)$ is the velocity of fluid, B the magnetic field, E the electric field, J the current density vector, μ_e the magnetic permeability, ε_e the absolute permittivity of the fluid, t denotes the time, ρ is the fluid density, T is the fluid temperature, C is the fluid concentration, ν is the kinematic viscosity, k is the thermal conductivity, D_m is the species concentration diffusiv-

ity, μ is the dynamic viscosity, g is the acceleration due to gravity, σ is the Stefan-Boltzmann constant, k^* is the Darcy permeability, T_m is the mean fluid temperature, k_1 is the reaction rate constant, β_T is the coefficient of thermal expansion, β_c is the coefficient of concentration expansion, C_p is the specific heat at constant pressure, C_s is the concentration susceptibility, and k_T is the thermal diffusion ratio.

We put also

$$B = (0, B_0, 0), \tag{11}$$

$$E = (E_x, E_y, E_z), \tag{12}$$

$$J = (J_x, 0, J_z), \tag{13}$$

where B_0 is a constant. We assumed that no applied polarization voltage exists (*i.e.*, $E = 0$). Then, Equation (10) and Equation (13) give

$$J = \sigma B_0 (-w, 0, u) \tag{14}$$

and Equation (9) yields

$$\nabla \cdot J = \sigma B_0 \left(\frac{\partial u}{\partial z} - \frac{\partial w}{\partial x} \right). \tag{15}$$

2.2. Physical Model

The flow is considered to be two-dimensional and steady, driven by free convection of an incompressible, viscous, and electrically conducting fluid past a semi-infinite vertical porous plate located at $y = 0$. The analysis takes into account thermal diffusion, viscous dissipation, heat absorption, and chemical reaction effects. The coordinate system is defined in such a way that the *x*-axis runs vertically along the plate, while the *y*-axis is perpendicular to it. A uniform magnetic field of intensity B_0 is applied in the *y*-direction. At the plate surface, the velocity, temperature, and concentration are held constant at $u = U_0$, $T = T_w$, and $C = C_w$, respectively. Far from the wall, the velocity is zero and the ambient fluid temperature and concentration approach (T_∞) and (C_∞), respectively. The physical configuration and coordinate system of the model are illustrated in Figure 1.

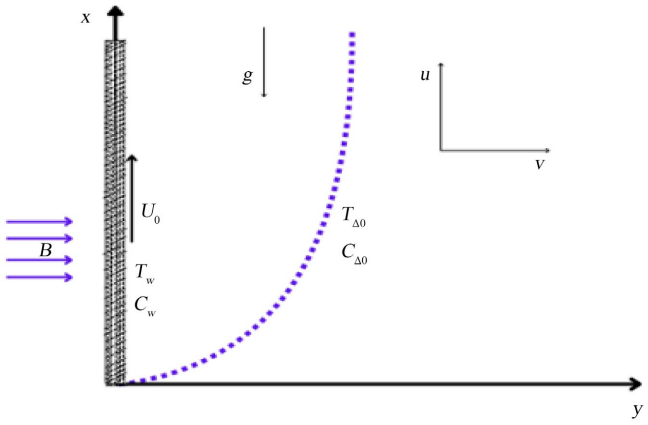

Figure 1. Physical model.

2.3. Governing Equations

Under Prandtl's assumptions and boundary layer approximations, the dimensional equations of continuity, momentum, energy, and concentration for steady fluid flow are given as follows:

$$\frac{\partial u}{\partial x}+\frac{\partial \upsilon}{\partial y}=0, \tag{16}$$

$$u\frac{\partial u}{\partial x}+\upsilon\frac{\partial u}{\partial y}=\nu\left(\frac{\partial^2 u}{\partial y^2}\right)+g\beta_T\left(T-T_\infty\right)+g\beta_c\left(C-C_\infty\right)-\frac{\nu}{k^*}u-\frac{\sigma B_0^2}{\rho}u, \tag{17}$$

$$u\frac{\partial T}{\partial x}+\upsilon\frac{\partial T}{\partial y}=\frac{k}{\rho C_p}\left(\frac{\partial^2 T}{\partial y^2}\right)+\frac{Q}{\rho C_p}\left(T-T_\infty\right)+\frac{D_m k_T}{C_s C_p}\left(\frac{\partial^2 C}{\partial y^2}\right)+\frac{\mu}{\rho C_p}\left(\frac{\partial u}{\partial y}\right)^2, \tag{18}$$

$$u\frac{\partial C}{\partial x}+\upsilon\frac{\partial C}{\partial y}=D_m\left(\frac{\partial^2 C}{\partial y^2}\right)-k_1\left(C-C_\infty\right)+\frac{D_m k_T}{T_m}\frac{\partial^2 T}{\partial y^2}, \tag{19}$$

with the boundary conditions:

$$\begin{cases} u=U_0,\ \upsilon=v_0,\ T=T_w,\ C=C_w & \text{at } y=0 \\ u=0,\ \upsilon=0,\ T\to T_\infty,\ C\to C_\infty & \text{at } y\to\infty. \end{cases} \tag{20}$$

The dimensionless governing equations were obtained by applying the following boundary layer approximations and dimensionless variables:

$$U=\frac{u}{U_O};\ V=\upsilon\Big/\left(U_0/\sqrt{R_e}\right);\ X=\frac{x}{L};\ Y=\frac{y}{\delta};$$

$$R_e=\frac{U_0 L}{\nu};\ \delta=\sqrt{\nu L/U_0};\ L=\frac{\delta^2 U_O}{\nu};$$

$$\frac{\delta}{L}=\frac{1}{\sqrt{R_e}};\ \frac{U_e}{L}=\frac{\nu}{\delta^2};\ T=T_\infty+\tilde{T}\left(T_w-T_\infty\right);$$

$$C=C_\infty+\tilde{C}\left(C_w-C_\infty\right);$$

with δ the maximum boundary layer thickness, L the plate length, R_e the hydrodynamic Reynolds number, X and Y the dimensionless coordinates.

Thus, we obtain the following dimensionless equations:

$$\frac{\partial U}{\partial X}+\frac{\partial V}{\partial Y}=0 \tag{21}$$

$$\begin{aligned} U\frac{\partial U}{\partial X}+V\frac{\partial U}{\partial Y}=&\frac{\partial^2 U}{\partial Y^2}+\frac{g\delta^2\beta_T\left(T_w-T_\infty\right)}{\nu U_0}\tilde{T}+\frac{g\delta^2\beta_c\left(C_w-C_\infty\right)}{\nu U_0}\tilde{C} \\ &-\frac{\delta^2}{k^*}U-\frac{\sigma B_O^2\delta^2}{\rho\nu}U \end{aligned} \tag{22}$$

$$\begin{aligned} U\frac{\partial\tilde{T}}{\partial X}+V\frac{\partial\tilde{T}}{\partial Y}=&\frac{k}{\nu\rho C_p}\frac{\partial^2\tilde{T}}{\partial Y^2}+\frac{Q\delta^2}{\rho C_p\nu}\tilde{T}+\frac{D_m k_T}{C_s C_p\nu}\frac{C_w-C_\infty}{T_w-T_\infty}\frac{\partial^2\tilde{C}}{\partial Y^2} \\ &+\frac{U_o^2}{C_p\left(T_w-T_\infty\right)}\left(\frac{\partial U}{\partial Y}\right)^2. \end{aligned} \tag{23}$$

$$U\frac{\partial\tilde{C}}{\partial X}+V\frac{\partial\tilde{C}}{\partial Y}=\frac{D_m}{\nu}\frac{\partial^2\tilde{C}}{\partial Y^2}-\frac{k_1\delta^2}{\nu}\tilde{C}+\frac{D_m k_T}{T_m\nu}\frac{T_w-T_\infty}{C_w-C_\infty}\frac{\partial^2\tilde{T}}{\partial Y^2}. \tag{24}$$

Taking the following dimensionless parameters:

$$S=\frac{Q\delta^2}{\rho C_p\nu};\ M=\frac{\sigma B_O^2\delta^2}{\rho\nu};\ S_c=\frac{\nu}{D_m};$$

$$S_r=\frac{D_m k_T}{T_m\nu}\frac{T_w-T_\infty}{C_w-C_\infty};\ k_p=\frac{\delta^2}{k^*};\ \gamma=\frac{k_1\delta^2}{\nu};\ P_r=\frac{\nu\rho C_p}{k};$$

$$E_c=\frac{U_o^2}{C_p\left(T_w-T_\infty\right)};\ G_r=\frac{g\delta^2\beta_T\left(T_w-T_\infty\right)}{\nu U_0};\ G_m=\frac{g\delta^2\beta_c\left(C_w-C_\infty\right)}{\nu U_0};$$

$$D_u=\frac{D_m k_T}{C_s C_p\nu}\frac{C_w-C_\infty}{T_w-T_\infty};$$

The dimensionless governing equations therefore become:

$$\frac{\partial U}{\partial X}+\frac{\partial V}{\partial Y}=0 \tag{25}$$

$$U\frac{\partial U}{\partial X}+V\frac{\partial U}{\partial Y}=\frac{\partial^2 U}{\partial Y^2}+G_r\tilde{T}+G_m\tilde{C}-k_pU-MU \tag{26}$$

$$U\frac{\partial\tilde{T}}{\partial X}+V\frac{\partial\tilde{T}}{\partial Y}=\frac{1}{P_r}\frac{\partial^2\tilde{T}}{\partial Y^2}+S\tilde{T}+D_u\frac{\partial^2\tilde{C}}{\partial Y^2}+E_c\left(\frac{\partial U}{\partial Y}\right)^2. \tag{27}$$

$$U\frac{\partial\tilde{C}}{\partial X}+V\frac{\partial\tilde{C}}{\partial Y}=\frac{1}{S_c}\frac{\partial^2\tilde{C}}{\partial Y^2}-\gamma\tilde{C}+S_r\frac{\partial^2\tilde{T}}{\partial Y^2}. \tag{28}$$

with the boundary conditions:

$$\begin{cases}U=1,\ V=V_0,\ \tilde{T}=1,\ \tilde{C}=1 & \text{at } Y=0\\ U=0,\ V=0,\ \tilde{T}\to 0,\ \tilde{C}\to 0 & \text{at } Y\to\infty,\end{cases} \tag{29}$$

where U, $\tilde{T}$ and $\tilde{C}$ represent the dimensionless velocity, temperature and concentration respectively, E_c is the Eckert number, G_r is the Grashof number, G_m is the modified Grashof number, S_c is the Schmidt number, S is the heat source parameter, P_r is the Prandlt number, k_p is the permeability of the porous medium, M is the magnetic parameter, D_u is the Dufour number, γ is the chemical reaction parameter and S_r is the Soret number.

2.4. Ordinary Differential Equations

The previous equations admit for the variables U, $\tilde{T}$ and $\tilde{C}$, the solutions, $U(X,Y)=f(\theta)$, $\tilde{T}(X,Y)=\tilde{T}(\theta)$ and $\tilde{C}(X,Y)=\tilde{C}(\theta)$ with $\theta=\frac{Y}{\sqrt{X}}$.

So we have:

$$\begin{cases}\dfrac{\partial U}{\partial X}=\dfrac{\partial f(\theta)}{\partial X}=\dfrac{\partial\theta}{\partial X}\dfrac{\mathrm{d}f(\theta)}{\mathrm{d}\theta}=-\dfrac{Y}{2X\sqrt{X}}\dfrac{\mathrm{d}f(\theta)}{\mathrm{d}\theta};\\ \dfrac{\partial\tilde{T}}{\partial X}=\dfrac{\partial\theta}{\partial X}\dfrac{\mathrm{d}\tilde{T}(\theta)}{\mathrm{d}\theta}=-\dfrac{Y}{2X\sqrt{X}}\dfrac{\mathrm{d}\tilde{T}(\theta)}{\mathrm{d}\theta};\\ \dfrac{\partial\tilde{C}}{\partial X}=\dfrac{\partial\theta}{\partial X}\dfrac{\mathrm{d}\tilde{C}(\theta)}{\mathrm{d}\theta}=-\dfrac{Y}{2X\sqrt{X}}\dfrac{\mathrm{d}\tilde{C}(\theta)}{\mathrm{d}\theta};\end{cases} \tag{30}$$

$$\begin{cases} \dfrac{\partial U}{\partial Y}=\dfrac{\partial f(\theta)}{\partial Y}=\dfrac{\partial \theta}{\partial Y}\dfrac{\mathrm{d}f(\theta)}{\mathrm{d}\theta}=\dfrac{1}{\sqrt{X}}\dfrac{\mathrm{d}f(\theta)}{\mathrm{d}\theta}; \\ \dfrac{\partial \tilde{T}}{\partial Y}=\dfrac{\partial \theta}{\partial Y}\dfrac{\mathrm{d}\tilde{T}(\theta)}{\mathrm{d}\theta}=\dfrac{1}{\sqrt{X}}\dfrac{\mathrm{d}\tilde{T}(\theta)}{\mathrm{d}\theta}; \\ \dfrac{\partial \tilde{C}}{\partial Y}=\dfrac{\partial \theta}{\partial Y}\dfrac{\mathrm{d}\tilde{C}(\theta)}{\mathrm{d}\theta}=\dfrac{1}{\sqrt{X}}\dfrac{\mathrm{d}\tilde{C}(\theta)}{\mathrm{d}\theta}; \end{cases} \tag{31}$$

$$\begin{cases} \dfrac{\partial^2 U}{\partial Y^2}=\dfrac{1}{X}\dfrac{\mathrm{d}^2 f(\theta)}{\mathrm{d}\theta^2}; \\ \dfrac{\partial^2 \tilde{T}}{\partial Y^2}=\dfrac{1}{X}\dfrac{\mathrm{d}^2 \tilde{T}(\theta)}{\mathrm{d}\theta^2}; \\ \dfrac{\partial^2 \tilde{C}}{\partial Y^2}=\dfrac{1}{X}\dfrac{\mathrm{d}^2 \tilde{C}(\theta)}{\mathrm{d}\theta^2}. \end{cases} \tag{32}$$

Thus, the continuity Equation (25) becomes:

$$\frac{\partial V}{\partial Y}=\frac{Y}{2X\sqrt{X}}\frac{\mathrm{d}f(\theta)}{\mathrm{d}\theta}$$

$$\Leftrightarrow \quad \mathrm{d}V=\frac{Y}{2X\sqrt{X}}\frac{\mathrm{d}f(\theta)}{\mathrm{d}\theta}\mathrm{d}Y.$$

As $Y=\theta\sqrt{X}$ and $\mathrm{d}Y=\sqrt{X}\mathrm{d}\theta$,

then:

$$\mathrm{d}V=\frac{X\theta}{2X\sqrt{X}}\frac{\mathrm{d}f(\theta)}{\mathrm{d}\theta}\mathrm{d}\theta$$

$$\Leftrightarrow \quad \mathrm{d}V=\frac{\theta}{2\sqrt{X}}\mathrm{d}f(\theta)$$

$$\Leftrightarrow \quad V(X,\theta)=\frac{1}{2\sqrt{X}}\int_0^\theta \varepsilon \mathrm{d}f(\varepsilon).$$

Integration by parts gives us:

$$V(X,\theta)=\frac{1}{2\sqrt{X}}\left[\theta f-\int_0^\theta f(\varepsilon)\mathrm{d}\varepsilon\right]. \tag{33}$$

If we introduce the function $F(\theta)=\int_0^\theta f(\varepsilon)\mathrm{d}\varepsilon$, Equation (33) becomes:

$$V(X,\theta)=\frac{1}{2\sqrt{X}}\left[\theta F'-F\right], \tag{34}$$

with

$$U=f=F'.$$

From the relations or systems of Equations (30)-(32) and (34), Equations (26)-(28) become respectively:

$$F'''+\frac{1}{2}F''F-\left(M+k_p\right)F'+G_r\tilde{T}+G_m\tilde{C}=0, \tag{35}$$

$$\tilde{T}''+\frac{1}{2}P_rF\tilde{T}'+E_cP_rF''^2+P_rS\tilde{T}+P_rD_u\tilde{C}''=0, \tag{36}$$

$$\tilde{C}'' + \frac{1}{2} S_c F \tilde{C}' - S_c \gamma \tilde{C} + S_c S_r \tilde{T}'' = 0, \tag{37}$$

with: $\frac{\mathrm{d}f}{\mathrm{d}\theta} = f' = F''$; $\frac{\mathrm{d}^2 f}{\mathrm{d}\theta^2} = f'' = F'''$; $\frac{\mathrm{d}\tilde{T}}{\mathrm{d}\theta} = \tilde{T}'$; $\frac{\mathrm{d}^2 \tilde{T}}{\mathrm{d}\theta^2} = \tilde{T}''$; $\frac{\mathrm{d}\tilde{C}}{\mathrm{d}\theta} = \tilde{C}'$; $\frac{\mathrm{d}^2 \tilde{C}}{\mathrm{d}\theta^2} = \tilde{C}''$.

The boundary conditions give:

$$\begin{cases} U = 1,\ V = -\alpha F_w,\ F = F_w,\ \tilde{T} = 1,\ \tilde{C} = 1 \quad \text{at } \theta = 0 \\ U = 0,\ \tilde{T} \to 0,\ \tilde{C} \to 0 \quad \text{at } \theta \to \infty, \end{cases} \tag{38}$$

with $\alpha > 0$.

The following non-dimensional quantities represent the skin friction coefficient (C_f), the Nusselt number (N_u) and the Sherwood number (S_h) respectively:

$$C_f = -\frac{1}{2\sqrt{2}} (G_r)^{\frac{3}{4}} \left(\frac{\mathrm{d}f}{\mathrm{d}\theta} \right)_{\theta=0}$$

$$N_u = \frac{1}{\sqrt{2}} (G_r)^{\frac{3}{4}} \left(\frac{\mathrm{d}\tilde{T}}{\mathrm{d}\theta} \right)_{\theta=0}$$

$$S_h = \frac{1}{\sqrt{2}} (G_r)^{\frac{3}{4}} \left(\frac{\mathrm{d}\tilde{C}}{\mathrm{d}\theta} \right)_{\theta=0}$$

3. Numerical Solution Method

For the numerical solution, we used the bvp4c technique, a solver integrated into MATLAB (Shampine *et al.* [23]). Thus, the highly coupled nonlinear ordinary differential Equations (35)-(37) with boundary conditions (38) are solved by defining:

$$A = 1 - P_r D_u S_c S_r; \quad A_1 = P_r / A;$$

$$A_2 = P_r S / A; \quad A_3 = P_r E_c / A;$$

$$A_4 = S_c D_u P_r / A; \quad A_5 = \gamma A_4;$$

$$A_6 = S_c / A; \quad A_7 = \gamma A_6;$$

$$A_8 = S_c S_r P_r / A; \quad A_9 = S_c S_r P_r S / A;$$

$$A_{10} = S_c S_r E_c P_r / A;$$

$$F = y_1; \quad F' = y_2; \quad F'' = y_3;$$

$$\tilde{T} = y_4; \quad \tilde{T}' = y_5;$$

$$\tilde{C} = y_6; \quad \tilde{C}' = y_7;$$

$$F''' = y_3' = -0.5 y_3 y_1 + (M + kp) y_2 - G_r y_4 - G_m y_6;$$

$$\tilde{T}'' = y_5' = -0.5 A_1 y_1 y_5, - A_2 y_4 - A_3 y_3^2 + 0.5 A_4 y_1 y_7 - A_5 y_6;$$

$$\tilde{C}'' = y_7' = -0.5 A_6 y_1 y_7 + A_7 y_6 + 0.5 A_8 y_1 y_5 + A_9 y_4 + A_{10} y_3^2.$$

For $\theta = 0$, $y_1 = 0$; $y_2 = 1$; $y_4 = 1$ and $y_6 = 1$.
For $\theta \to \infty$, $y_2 = 0$; $y_4 = 0$ and $y_6 = 0$.

4. Results and Discussions

The numerical results of the present study were obtained for various parameter values affecting velocity, temperature, concentration, wall friction coefficient, Nusselt number, and Sherwood number across a moving vertical porous permeable plate, using the bvp4c method in MATLAB.

These results were computed for different values of the porous medium permeability parameter (k_p), Eckert number (E_c), Soret number (S_r), magnetic parameter (M), Schmidt number (S_c), Prandtl number (P_r), heat source parameter (S), chemical reaction parameter (γ), Grashof number (G_r), modified Grashof number (G_m), Dufour number (D_u), injection/suction rate, and the plate movement rate, and are presented in Figures 2-16.

In the numerical solution process, to obtain the results shown in the figures and tables, the following default parameter values were defined: $M = 1.0$, $G_r = 10$; $G_m = 5$; $\gamma = 0.50$; $k_p = 1.0$; $S_r = 1.0$; $S = 0.10$; $P_r = 0.63$; $E_c = 0.01$; $D_u = 0.5$; $S_c = 0.22$; $F_w = 0$. In each case, θ is along the horizontal axis.

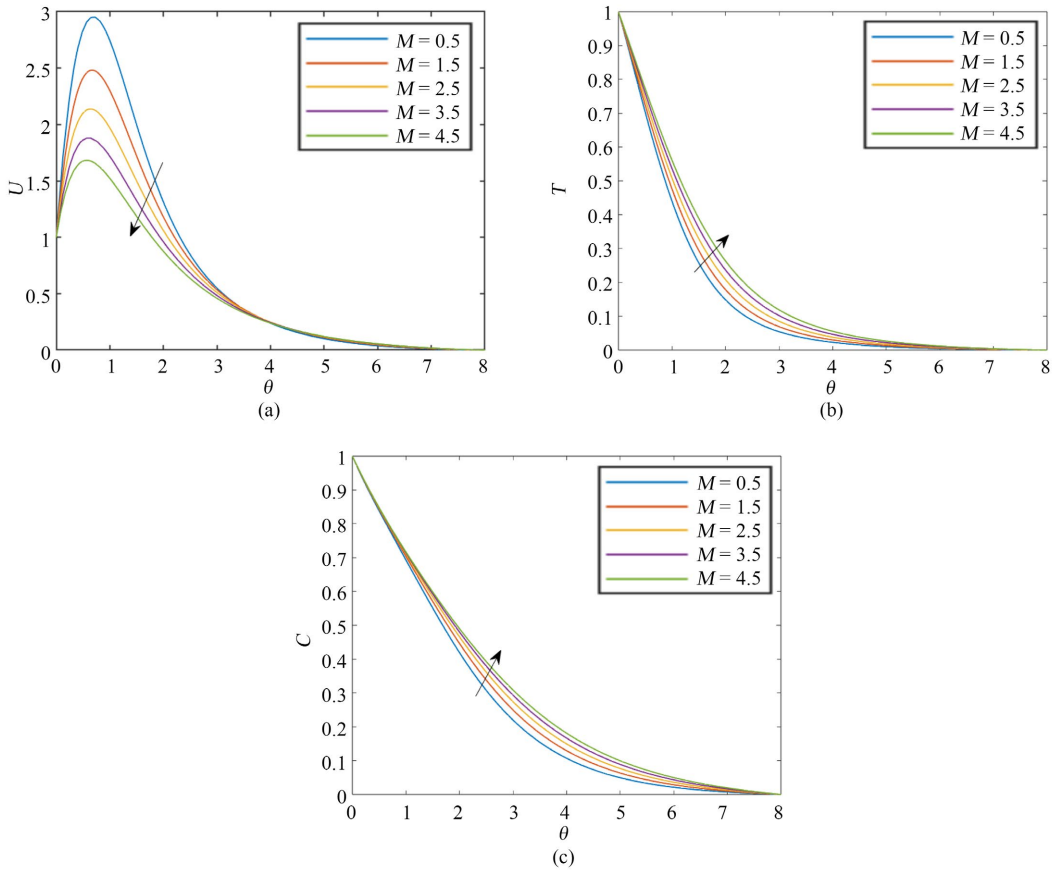

Figure 2. (a) Velocity profiles, (b) temperature profiles and (c) concentration profiles for different values of M against θ.

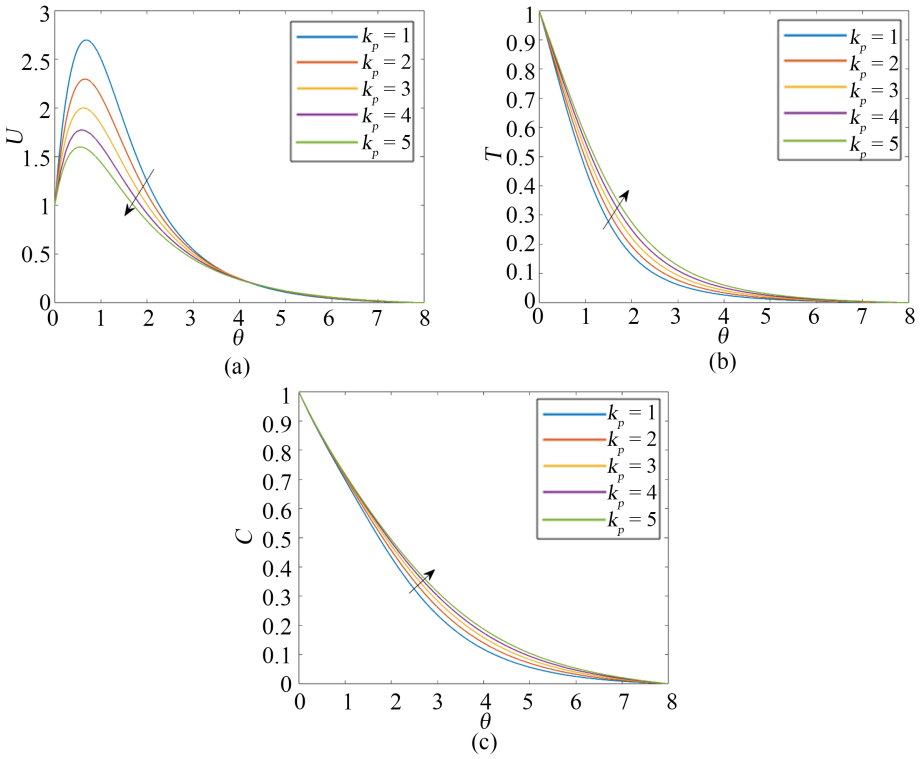

Figure 3. (a) Velocity profiles, (b) temperature profiles and (c) concentration profiles for different values of k_p against θ.

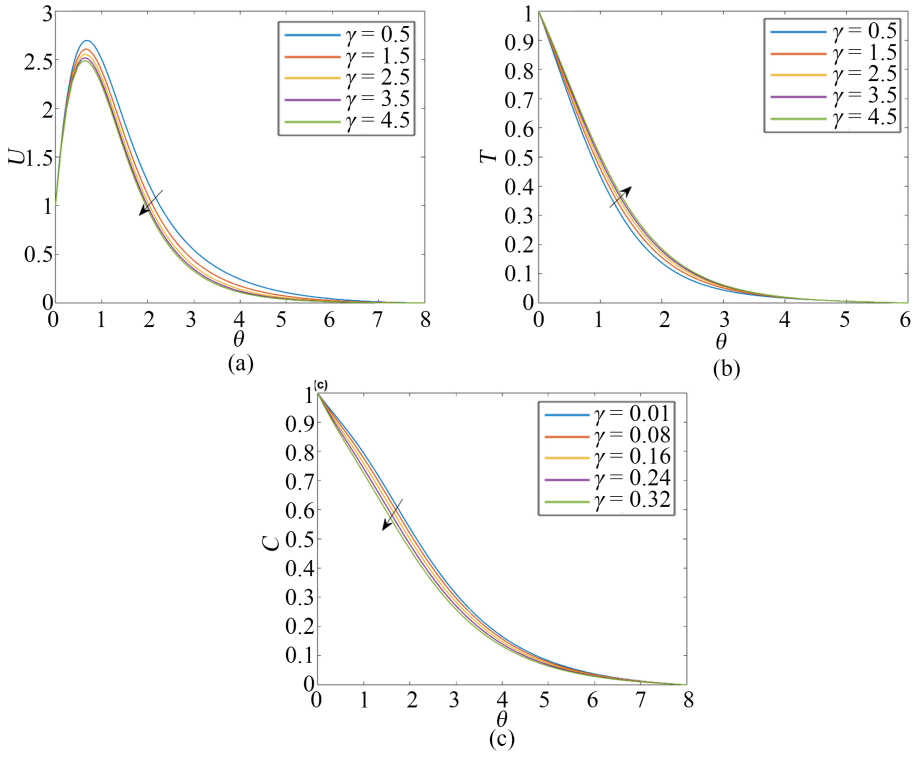

Figure 4. (a) Velocity profiles, (b) temperature profiles and (c) concentration profiles for different values of γ against θ.

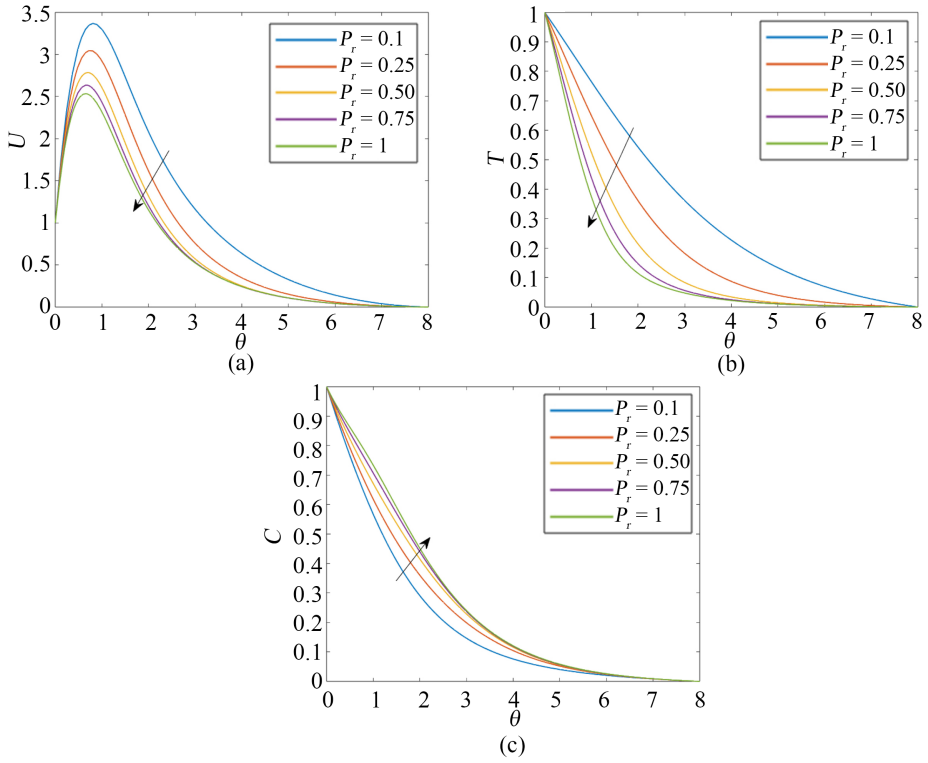

Figure 5. (a) Velocity profiles, (b) temperature profiles and (c) concentration profiles for different values of P_r against θ.

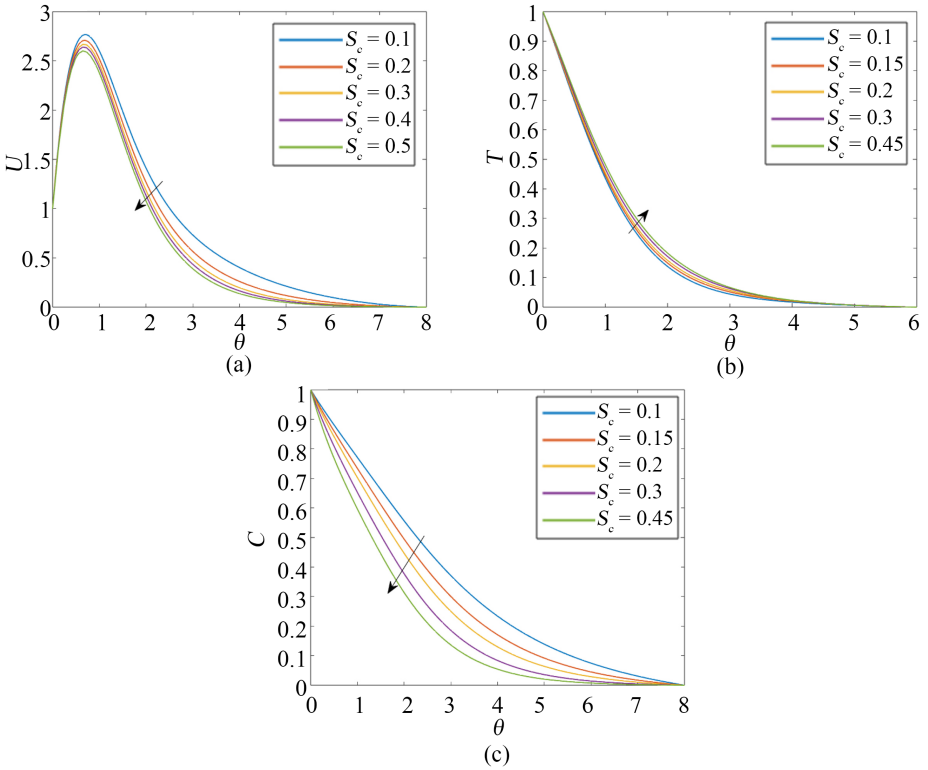

Figure 6. (a) Velocity profiles, (b) temperature profiles and (c) concentration profiles for different values of S_c against θ.

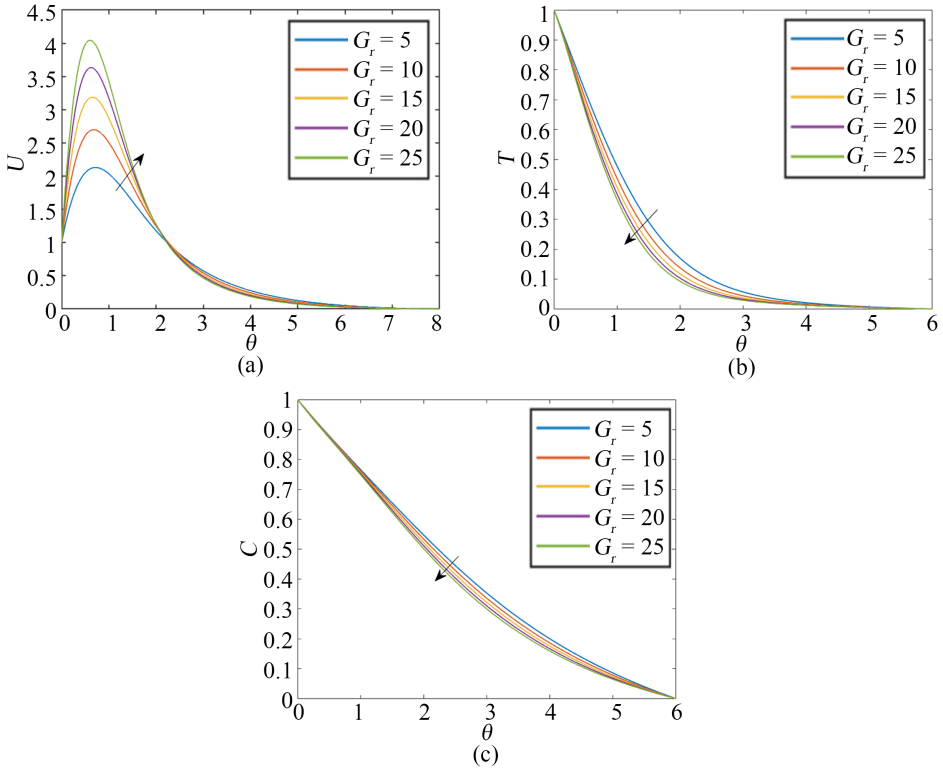

Figure 7. (a) Velocity profiles, (b) temperature profiles and (c) concentration profiles for different values of G_r against θ.

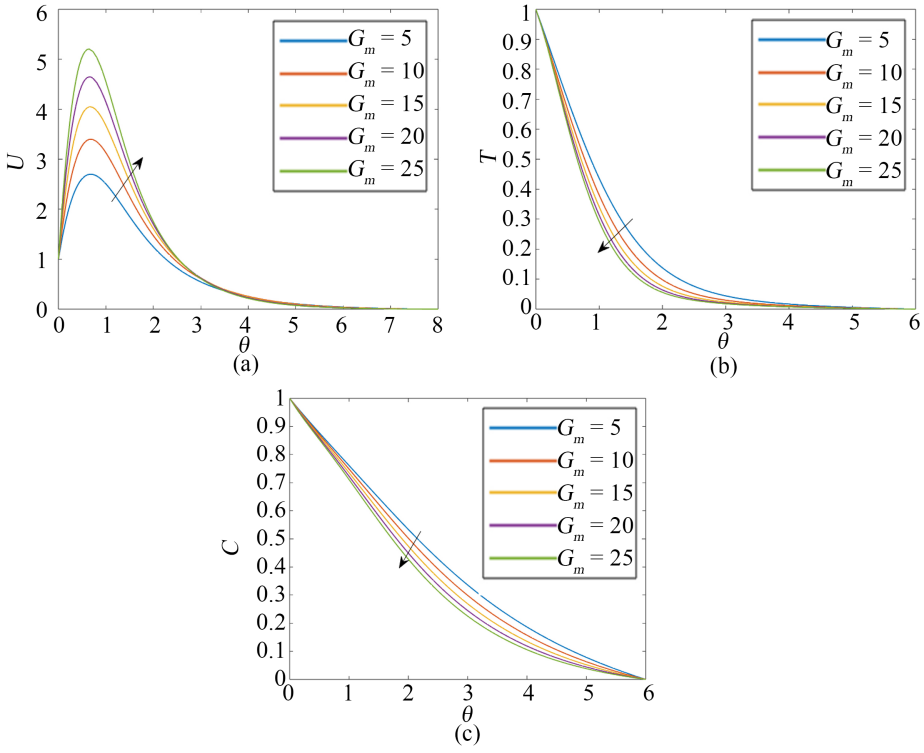

Figure 8. (a) Velocity profiles, (b) temperature profiles and (c) concentration profiles for different values of G_m against θ.

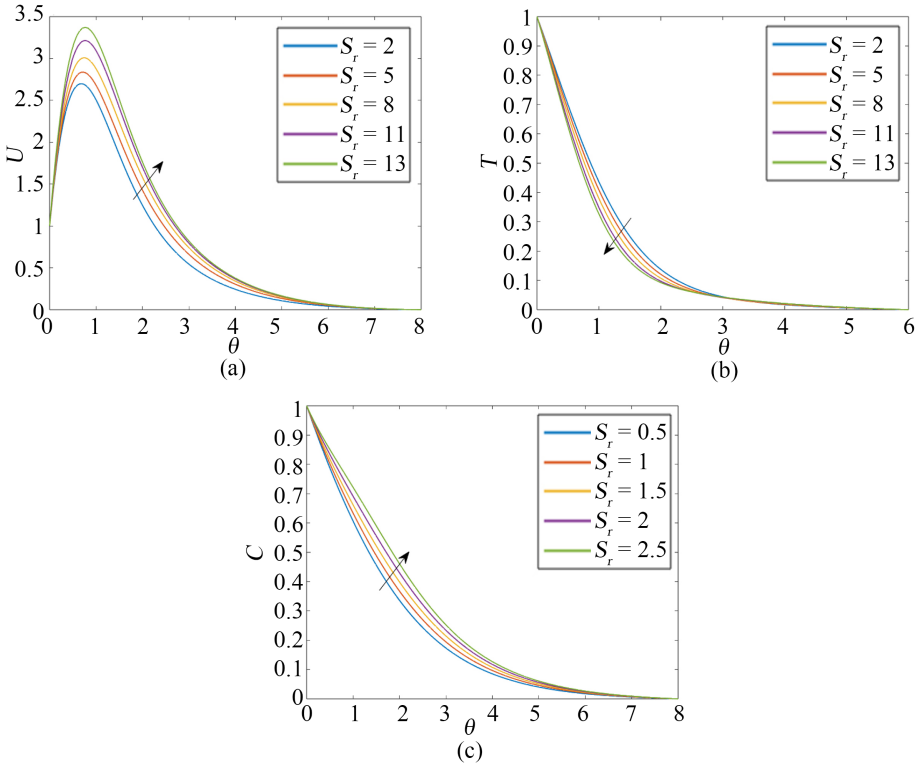

Figure 9. (a) Velocity profiles, (b) temperature profiles and (c) concentration profiles for different values of Sr against θ.

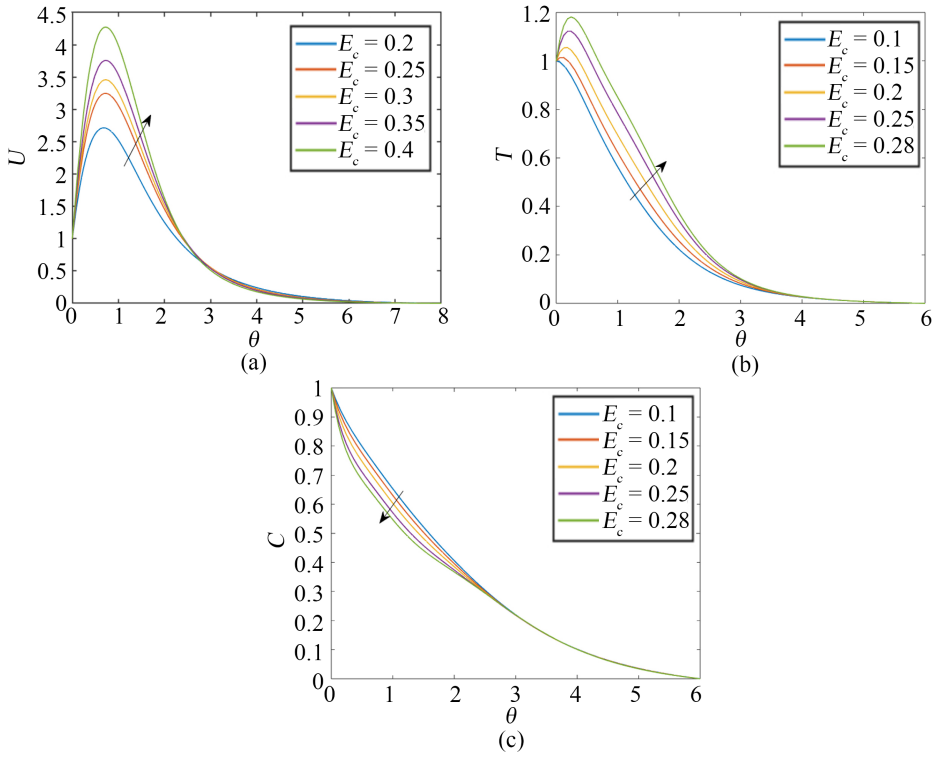

Figure 10. (a) Velocity profiles, (b) temperature profiles and (c) concentration profiles for different values of E_c against θ.

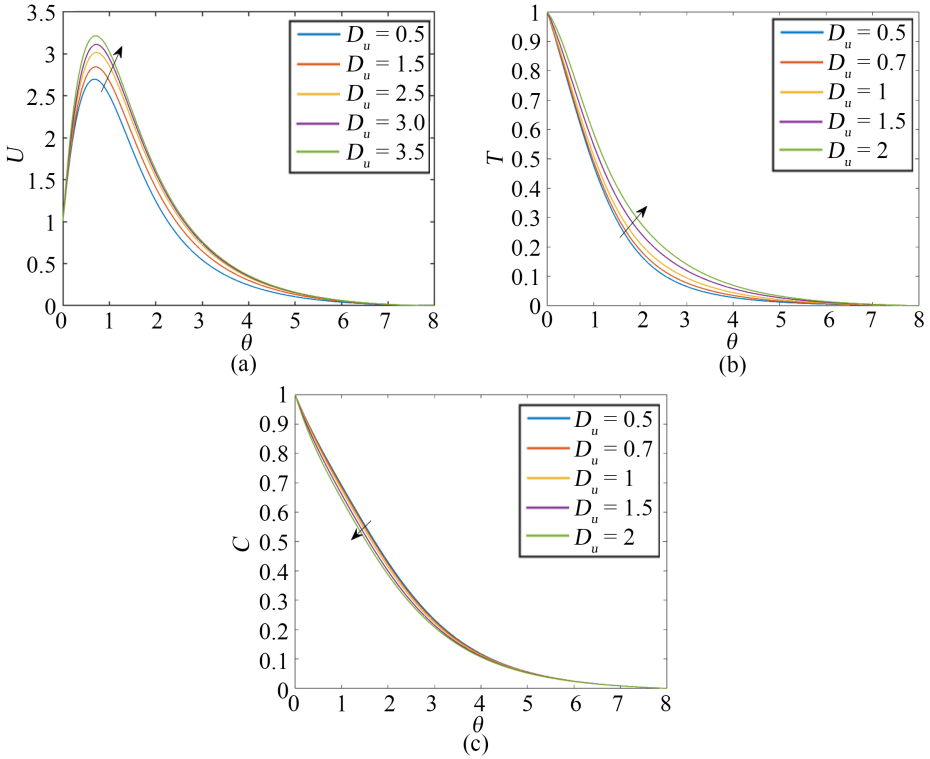

Figure 11. (a) Velocity profiles, (b) temperature profiles and (c) concentration profiles for different values of D_u against θ.

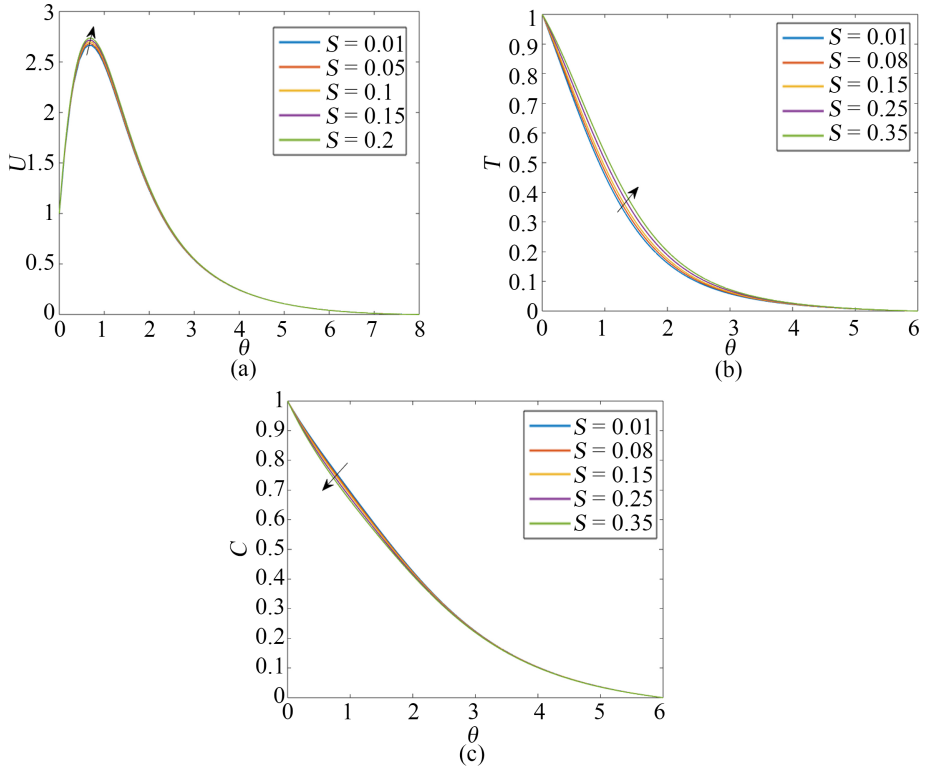

Figure 12. (a) Velocity profiles, (b) temperature profiles and (c) concentration profiles for different values of S against θ.

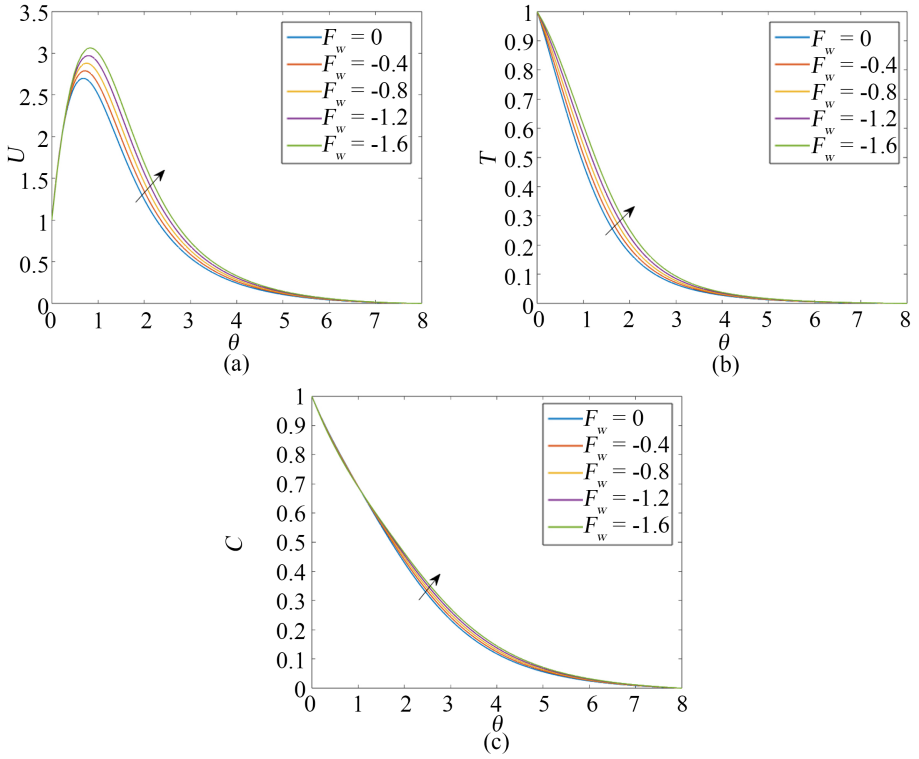

Figure 13. (a) Velocity profiles, (b) temperature profiles and (c) concentration profiles for different values of blowing velocity against θ.

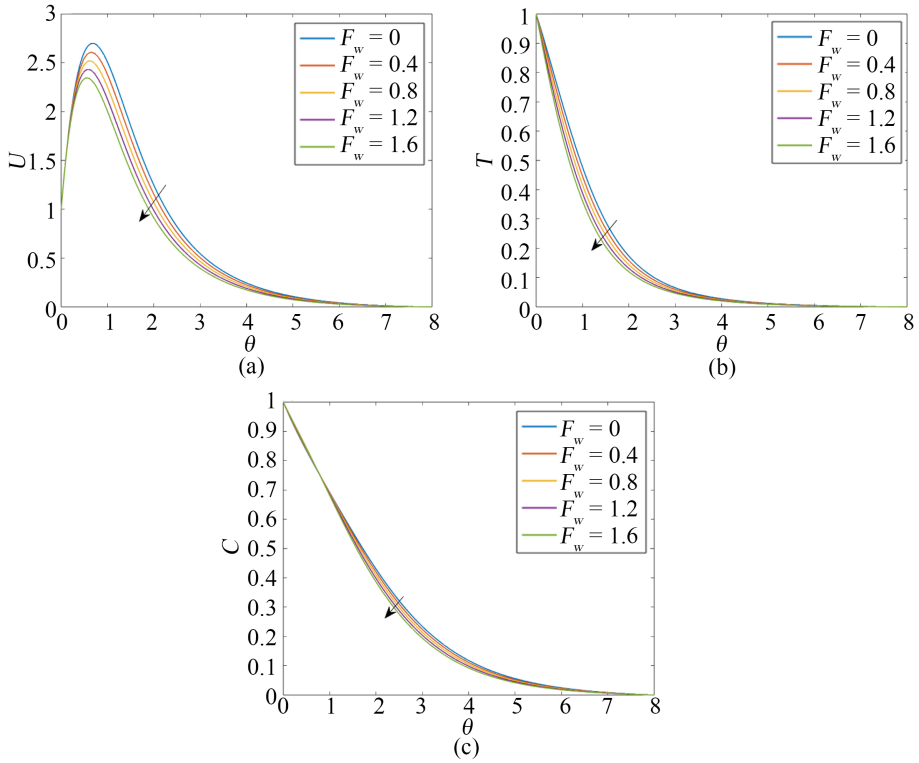

Figure 14. (a) Velocity profiles, (b) temperature profiles and (c) concentration profiles for different values of suction velocity against θ.

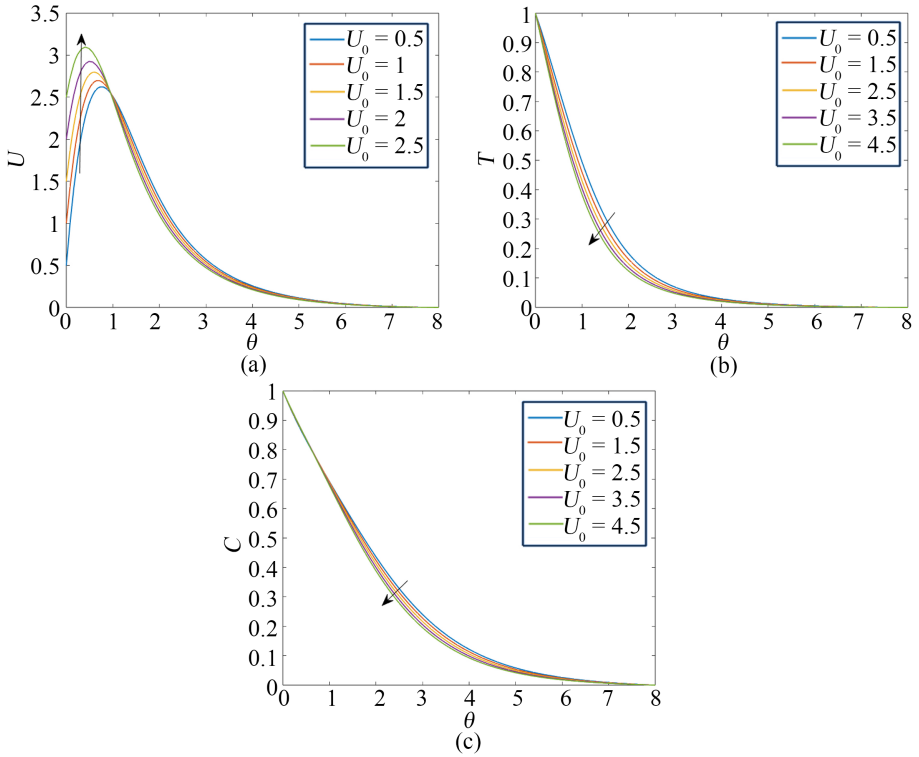

Figure 15. (a) Velocity profiles, (b) temperature profiles and (c) concentration profiles for different positive values of U_0 against θ.

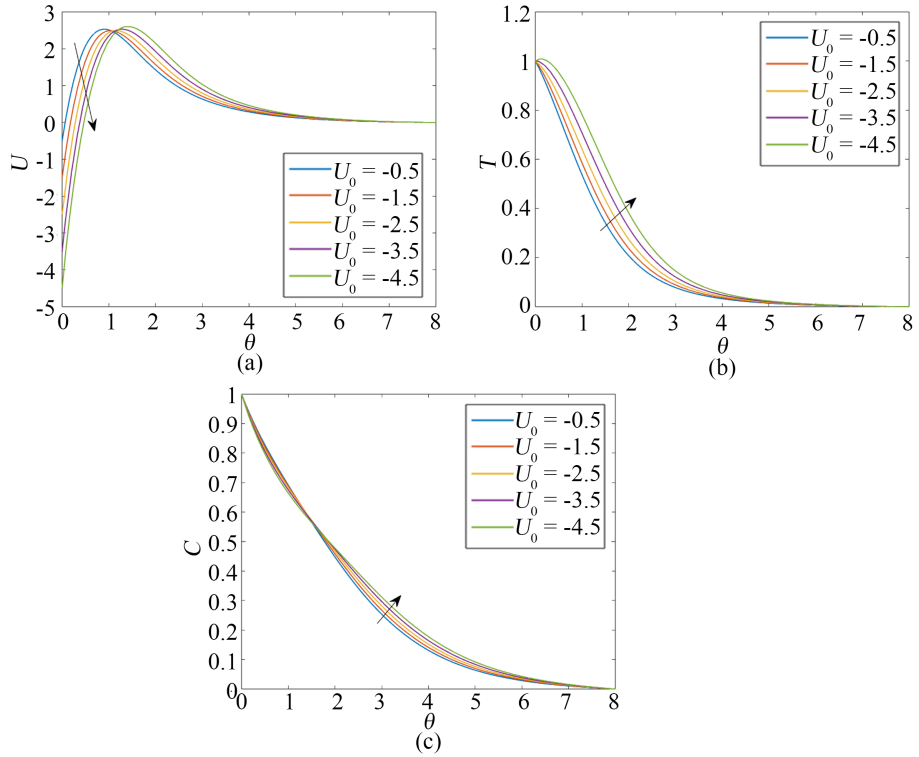

Figure 16. (a) Velocity profiles, (b) temperature profiles and (c) concentration profiles for different negative values of U_0 against θ.

Figure 2 illustrates the variations in velocity, temperature, and concentration profiles under the influence of different values of the magnetic parameter (M). An increase in the magnetic parameter M results in a gradual decrease in the fluid velocity (Figure 2(a)). This behavior is attributed to the generation of a resistive Lorentz force within the fluid, which acts to oppose the motion and thereby reduces the velocity profile. Conversely, increasing the magnetic parameter enhances both the temperature and concentration profiles (Figure 2(b) and Figure 2(c)), due to the additional energy dissipation and reduced convective transport.

Similarly, an increase in the permeability parameter (k_p) leads to a decrease in the fluid velocity profiles (Figure 3(a)), while increasing the temperature (Figure 3(b)) and concentration profiles (Figure 3(c)). This behavior can be attributed to the presence of the porous medium, which introduces an additional resistive force in the fluid flow. This resistance reduces the velocity distribution and, in turn, enhances the temperature and concentration distributions.

Figure 4 illustrates the effect of the chemical reaction parameter (γ) on the velocity, temperature, and concentration profiles. As shown, the velocity (Figure 4(a)) and concentration (Figure 4(c)) decrease with an increase in the chemical reaction parameter (γ). In contrast, the temperature (Figure 4(b)) increases as γ increases. Physically, this behavior can be attributed to the fact that positive values of the chemical reaction parameter ($\gamma > 0$) correspond to a destructive chemical reaction, which reduces the concentration of the reactive species and, consequently, the flow velocity.

As for the Prandtl number (P_r) shown in Figure 5, an increase in P_r significantly decreases the velocity (Figure 5(a)) and temperature (Figure 5(b)), while increasing the concentration of fluid particles (Figure 5(c)). This behavior is expected, as fluids with higher Prandtl numbers possess greater viscosity, which reduces the flow velocity and decreases the thickness of the thermal boundary layer. Consequently, a thinner thermal boundary layer leads to reduced heat transfer.

In Figure 6, the velocity, temperature, and concentration profiles are influenced by the Schmidt number (S_c). As S_c increases, the concentration of nanoparticles (Figure 6(c)) decreases, which in turn leads to a reduction in the velocity profiles (Figure 6(a)), while the temperature profiles exhibit a slight increase (Figure 6(b)). Physically, the Schmidt number (S_c) is a dimensionless parameter defined as the ratio of momentum diffusivity (viscous diffusivity) to mass diffusivity. Therefore, an increase in S_c implies lower mass diffusivity, which restricts mass transport and results in decreased concentration and velocity profiles.

Figure 7 and Figure 8 illustrate the effects of the Grashof number (G_r) and the modified Grashof number (G_m) on the velocity, temperature, and concentration profiles, respectively. It is observed that increasing either G_r (Figure 7) or G_m (Figure 8) significantly enhances the velocity profiles (Figure 7(a) and Figure 8(a)). However, this increase in buoyancy-driven flow leads to a reduction in both temperatures (Figure 7(b) and Figure 8(b)) and concentration profiles (Figure 7(c) and Figure 8(c)). Physically, the Grashof number represents the ratio of buoy-

ancy to viscous forces within the boundary layer. A higher Grashof number indicates stronger thermal buoyancy effects, which enhance fluid motion due to gravitational forces acting on density variations. As a result, the flow accelerates, leading to increased velocities, while the enhanced mixing and thinning of the thermal and concentration boundary layers contribute to the observed decreases in temperature and concentration profiles.

The effects of the Soret number (S_r) are illustrated in **Figure 9**. An increase in S_r leads to higher velocity and concentration profiles, as shown in **Figure 9(a)** and **Figure 9(c)**, respectively. This enhancement is due to the Soret effect, which describes mass flux induced by temperature gradients. As S_r increases, it promotes the diffusion of species from regions of higher temperature to lower temperature, thereby enhancing both fluid motion and species concentration. Consequently, the dynamic and concentration boundary layers become thicker. Conversely, the temperature profile (**Figure 9(b)**) decreases with increasing S_r, indicating a reduction in the thermal boundary layer thickness.

The effects of the Eckert number (E_c) on the velocity, temperature, and concentration profiles are presented in **Figure 10**. As observed in **Figure 10(a)** and **Figure 10(b)**, both the fluid velocity and temperature increase with rising E_c. This behavior is attributed to the conversion of kinetic energy into internal energy due to viscous dissipation, which enhances thermal energy within the fluid. As a result, the temperature rises and the flow accelerates. However, an increase in the Eckert number slightly reduces the concentration profile (**Figure 10(c)**), likely due to the dominance of thermal effects over mass diffusion in the flow field.

In **Figure 11**, an increase in the Dufour number D_u leads to higher velocity (**Figure 11(a)**) and temperature (**Figure 11(b)**) profiles. Conversely, a slight decrease is observed in the concentration profile (**Figure 11(c)**).

From **Figure 12**, it is observed that an increase in the heat source parameter (S) slightly enhances the velocity (**Figure 12(a)**) and temperature (**Figure 12(b)**) profiles. However, this increase in S leads to a slight reduction in the concentration of fluid particles (**Figure 12(c)**).

The effects of injection and suction velocities are illustrated in **Figure 13** and **Figure 14**, respectively. When the plate is subjected to an injection velocity, an increase in this velocity leads to higher flow velocity, temperature, and concentration profiles of the fluid particles. In other words, increasing the initial negative values of the stream function (F_w) enhances the velocity, temperature, and concentration distributions (**Figure 13**), thereby thickening the corresponding boundary layers. Conversely, when the plate is subjected to a suction velocity, an increase in this velocity results in a reduction in the flow velocity, temperature, and concentration profiles. That is, increasing the initial positive values of the stream function (F_w) diminishes these profiles (**Figure 14**), effectively thinning the boundary layers.

Figure 15 illustrates that increasing the plate's motion speed in the direction of the fluid flow enhances the initial flow velocity U_0, thereby increasing the flow

velocity profiles near the wall (Figure 15(a)). This increase in plate speed leads to a slight reduction in both the temperature (Figure 15(b)) and concentration (Figure 15(c)) profiles. In contrast, when the plate moves in the opposite direction of the fluid flow (Figure 16), increasing its speed gradually decreases the initial flow velocity U_0 and, consequently, reduces the flow velocity profiles near the wall (Figure 16(a)). This reverse motion results in a slight increase in the temperature (Figure 16(b)) and concentration (Figure 16(c)) profiles.

Tables 1-3 illustrate the effects of various parameters on the skin friction coefficient, Nusselt number, and Sherwood number for $\theta = 0.6867$. An increase in M or k_p (Table 1), or S_c or γ (Table 2), leads to a decrease in both the skin friction coefficient and the Nusselt number, while the Sherwood number increases. Conversely, increasing E_c (Table 1), D_u or S (Table 2), or U_0^- or F_w^- (Table 3) results in higher skin friction and Sherwood numbers but a lower Nusselt number. An increase in P_r (Table 1), or U_0^+ or F_w^+ (Table 3) reduces the skin friction and Sherwood numbers, while enhancing the Nusselt number. Increasing G_r (Table 1) raises the skin friction coefficient, but reduces both the Nusselt and Sherwood numbers. Similarly, an increase in S_r (Table 2) enhances the skin friction coefficient and Nusselt number, but decreases the Sherwood number. It is important to note that F_w^+ denotes the suction velocity, F_w^- the injection velocity, U_0^+ the plate velocity in the direction of the fluid flow, and U_0^- the plate velocity opposite to the fluid flow direction. Table 4 shows the results of R. Biswas *et al.* [24], and Table 5 shows the results of our work. After comparing these two tables, we notice that our work is in good agreement and represents the complement of the work of R. Biswas *et al.* [24].

Table 1. Effects of different parameters (M, k_p, G_r, P_r, E_c) on skin friction coefficient, Nusselt number and Sherwood number.

M	k_p	G_r	P_r	E_c	C_f	N_u	S_h
0.50					0.036612	0.308713	0.315315
0.70					0.030986	0.308679	0.315318
0.90					0.025428	0.308644	0.315320
	1.0				0.036612	0.308713	0.315315
	1.5				0.022674	0.308627	0.315322
	2.0				0.009143	0.308540	0.315330
		5			0.036612	0.308713	0.315315
		10			0.089843	0.183843	0.187506
		15			0.116425	0.135713	0.138411
			0.63		0.036612	0.308713	0.315315
			0.71		0.036581	0.308832	0.315264
			1.00		0.036460	0.309322	0.315050
				0.01	0.036612	0.308713	0.315315
				0.02	0.036681	0.307826	0.315704
				0.03	0.036750	0.306940	0.316092

Table 2. Effects of different parameters (D_u, S_c, γ, S_r, S) on skin friction coefficient, Nusselt number and Sherwood number.

D_u	S_c	γ	S_r	S	C_f	N_u	S_h
0.5					0.036612	0.308713	0.315315
0.0					0.036740	0.305505	0.316722
0.5					0.036928	0.300783	0.318793
	0.22				0.036612	0.308713	0.315315
	0.60				0.035641	0.302353	0.335455
	0.78				0.034893	0.297348	0.351308
		0.5			0.036612	0.308713	0.315315
		1.5			0.036007	0.304871	0.327477
		2.5			0.035417	0.301090	0.339450
			2		0.036612	0.308713	0.315315
			3		0.036679	0.308782	0.315107
			4		0.036758	0.308865	0.314856
				0.01	0.036612	0.308713	0.315315
				0.02	0.036756	0.305173	0.316868
				0.03	0.036902	0.301617	0.318427

Table 3. Effects of different parameters (U_0^-, U_0^+, F_w^+, F_w^-) on skin friction coefficient, Nusselt number and Sherwood number.

U_0^-	U_0^+	F_w^+	F_w^-	C_f	N_u	S_h
−0.4				0.306284	0.300423	0.316289
−0.8				0.380453	0.297138	0.316959
−1.0				0.417056	0.295350	0.317356
	0.4			0.154100	0.305790	0.315463
	0.8			0.076092	0.307846	0.315318
	1.0			0.036612	0.308713	0.315315
		0		0.036612	0.308713	0.315315
		0.4		0.028334	0.322734	0.313796
		0.8		0.019527	0.337212	0.312062
			0	0.036612	0.308713	0.315315
			−0.4	0.044362	0.295148	0.316620
			−0.8	0.051593	0.282039	0.317709

Table 4. Represents the previous results by R. Biswas *et al.* [24].

Parameters	U	$\tilde{T}$	$\tilde{C}$	C_f	N_u	S_h
M	↓			↓		
k_p	↓			↓		
G_r	↑			↑	↓	↓
P_r		↓		↓	↑	
E_c		↑				
S_c			↓	↓	↓	↑
γ	↓		↓		↓	↑
S_r	↑			↑		
S	↑	↑				

Table 5. Represents the present results.

Parameters	U	$\tilde{T}$	$\tilde{C}$	C_f	N_u	S_h
M	↓	↑	↑	↓		
k_p	↓	↑	↑	↓		
G_r	↑	↓	↓	↑	↓	↓
P_r	↓	↓	↑	↓	↑	
E_c	↑	↑	↓	↑	↓	↑
S_c	↓	↑	↓	↓	↓	↑
γ	↓	↑	↓		↓	↑
S_r	↑	↓	↑	↑		
S	↑	↑	↓	↑	↓	↑

5. Conclusions

From the above study, it is noted that:

1) Increasing the magnetic parameter M or the permeability parameter k_p improves the temperature and concentration profiles as well as the Sherwood number, but reduces the velocity profiles and deteriorates the skin friction coefficient and the Nusselt number.

2) Increasing the Schmidt number S_c or the chemical reaction parameter γ decreases the skin friction coefficient and the Nusselt number, as well as the velocity and concentration profiles, but improves the Sherwood number and the temperature profiles.

3) Increasing the Eckert number or Dufour number or the heat source param-

eter improves the velocity and temperature profiles as well as the skin friction coefficient and Sherwood number, but decreases the concentration profiles and the Nusselt number.

4) The movement of the plate in the direction of fluid flow increases the fluid velocity and the Nusselt number and reduces the temperature and concentration profiles, as well as the skin friction coefficient and the Sherwood number. On the other hand, the movement of the plate in the opposite direction of fluid flow has an opposite effect on these profiles.

5) Injection speed increases the velocity, temperature, and concentration profiles, as well as the skin friction coefficient and Sherwood number, but worsens the Nusselt number. In contrast, suction speed has the opposite effect on these profiles.

6) The Grashof number or modified Grashof number improves the velocity profiles and the skin friction coefficient, but decreases the temperature and concentration profiles, as well as the Nusselt number and the Sherwood number.

7) The Soret number S_r increases the particle velocity and concentration as well as the skin friction coefficient and the Nusselt number, but decreases the temperature and the Sherwood number.

8) The Prandlt number decreases the velocity and temperature profiles as well as the skin friction coefficient and the Sherwood number, but increases the concentration and the Nusselt number.

Conflicts of Interest

The authors declare no conflicts of interest regarding the publication of this paper.

References

[1] Hossain, M.D., Samad, M.A. and Alam, M.M. (2015) MHD Free Convection and Mass Transfer Flow through a Vertical Oscillatory Porous Plate with Hall, Ion-Slip Currents and Heat Source in a Rotating System. *Procedia Engineering*, **105**, 56-63. https://doi.org/10.1016/j.proeng.2015.05.006

[2] Khan, I., Hussain, A., Malik, M.Y. and Mukhtar, S. (2020) On Magnetohydrodynamics Prandtl Fluid Flow in the Presence of Stratification and Heat Generation. *Physica A*: *Statistical Mechanics and Its Applications*, **540**, Article ID: 123008. https://doi.org/10.1016/j.physa.2019.123008

[3] Zeb, S., Ullah, Z., Albidah, A.B., Khan, I. and Khan, W.A. (2025) The Significance of Heat Transfer through Natural Convection in Stagnation Point Flow of Prandtl Fluid. *Results in Physics*, **68**, Article ID: 108087. https://doi.org/10.1016/j.rinp.2024.108087

[4] Bilal, M. and Ashbar, S. (2020) Flow and Heat Transfer Analysis of Eyring-Powell Fluid over Stratified Sheet with Mixed Convection. *Journal of the Egyptian Mathematical Society*, **28**, Article No. 40. https://doi.org/10.1186/s42787-020-00103-6

[5] Awais, M., Bilal, S., Ur Rehman, K. and Malik, M.Y. (2020) Numerical Investigation of MHD Prandtl Melted Fluid Flow Towards a Cylindrical Surface: Comprehensive Outcomes. *Canadian Journal of Physics*, **98**, 223-232. https://doi.org/10.1139/cjp-2018-0582

[6] Al-Khafajy, D.G.S. and Al-Kaabi, W.A.M. (2021) Oscillatory Flow and Variable Vis-

cosity by the Heat for the Prandtl-Eyring Fluid through Porous Channel. *Journal of Physics*: *Conference Series*, **1999**, Article ID: 012095. https://doi.org/10.1088/1742-6596/1999/1/012095

[7] Alizadeh, R., Gomari, S.R., Alizadeh, A., Karimi, N. and Li, L.K.B. (2021) Combined Heat and Mass Transfer and Thermodynamic Irreversibilities in the Stagnation-Point Flow of Casson Rheological Fluid over a Cylinder with Catalytic Reactions and Inside a Porous Medium under Local Thermal Nonequilibrium. *Computers & Mathematics with Applications*, **81**, 786-810. https://doi.org/10.1016/j.camwa.2019.10.021

[8] Ibrahim, W. and Hindebu, B. (2019) Magnetohydrodynamic(MHD) Boundary Layer Flow of Eyring-Powell Nanofluid Past Stretching Cylinder with Cattaneo-Christov Heat Flux Model. *Nonlinear Engineering*, **8**, 303-317. https://doi.org/10.1515/nleng-2017-0167

[9] Layek, G.C., Mandal, B. and Bhattacharyya, K. (2020) Dufour and Soret Effects on Unsteady Heat and Mass Transfer for Powell-Eyring Fluid Flow over an Expanding Permeable Sheet. *Journal of Applied and Computational Mechanics*, **6**, 985-998.

[10] Jabeen, I., Farooq, M., Rizwan, M., Ullah, R. and Ahmad, S. (2014) Analysis of Nonlinear Stratified Convective Flow of Powell-Eyring Fluid: Application of Modern Diffusion. *Advances in Mechanical Engineering*, **12**. https://doi.org/10.1177/1687814020959568

[11] Salah, F. (2022) Chemical Reaction and Generalized Heat Flux Model for Powell-Eyring Model with Radiation Effects. *International Journal of Mathematics and Mathematical Sciences*, **2022**, Article ID: 4076426. https://doi.org/10.1155/2022/4076426

[12] Naseem, T., Bibi, I., Shahzad, A. and Munir, M. (2023) Analysis of Heat Transport in a Powell-Eyring Fluid with Radiation and Joule Heating Effects via a Similarity Transformation. *Fluid Dynamics & Materials Processing*, **19**, 663-677. https://doi.org/10.32604/fdmp.2022.021136

[13] Anwar, M.S., Alqarni, M.S. and Irfan, M. (2024) Exploring the Marvels of Heat Transfer: MHD Convection at a Stagnation Point in Non-Newtonian Fluid with Yield Stress and Chemical Reactions. *Chinese Journal of Physics*, **89**, 1299-1308. https://doi.org/10.1016/j.cjph.2024.01.030

[14] Jalili, P., Azar, A.A., Jalili, B. and Ganji, D.D. (2023) Study of Nonlinear Radiative Heat Transfer with Magnetic Field for Non-Newtonian Casson Fluid Flow in a Porous Medium. *Results in Physics*, **48**, Article ID: 106371. https://doi.org/10.1016/j.rinp.2023.106371

[15] Usman, Khan, W., Badruddin, I.A., Ghaffari, A. and Ali, H.M. (2021) Heat Transfer in Steady Slip Flow of Tangent Hyperbolic Fluid over the Lubricated Surface of a Stretchable Rotatory Disk. *Case Studies in Thermal Engineering*, **24**, Article ID: 100825. https://doi.org/10.1016/j.csite.2020.100825

[16] Biswas, R., Mondal, M., Sarkar, D. and Ahmmed, S. (2017) Effects of Radiation and Chemical Reaction on MHD Unsteady Heat and Mass Transfer of Casson Fluid Flow Past a Vertical Plate. *Journal of Advances in Mathematics and Computer Science*, **23**, 1-16. https://doi.org/10.9734/jamcs/2017/34292

[17] Ahmed, N., Khan, U., Khan, S.I., Bano, S. and Mohyud-Din, S.T. (2017) Effects on Magnetic Field in Squeezing Flow of a Casson Fluid between Parallel Plates. *Journal of King Saud University—Science*, **29**, 119-125. https://doi.org/10.1016/j.jksus.2015.03.006

[18] Meenakumari, R., Lakshminarayana, P. and Vajravelu, K. (2020) Influence of Induced Magnetic Field and Slip Conditions on Convective Prandtl Fluid Flow over a

Stretching Surface with Homogeneous and Heterogeneous Reactions. *Multidiscipline Modeling in Materials and Structures*, **17**, 127-147. https://doi.org/10.1108/mmms-02-2020-0040

[19] Kataria, H.R. and Patel, H.R. (2018) Effect of Thermo-Diffusion and Parabolic Motion on MHD Second Grade Fluid Flow with Ramped Wall Temperature and Ramped Surface Concentration. *Alexandria Engineering Journal*, **57**, 73-85. https://doi.org/10.1016/j.aej.2016.11.014

[20] Kataria, H.R. and Patel, H.R. (2016) Soret and Heat Generation Effects on MHD Casson Fluid Flow Past an Oscillating Vertical Plate Embedded through Porous Medium. *Alexandria Engineering Journal*, **55**, 2125-2137. https://doi.org/10.1016/j.aej.2016.06.024

[21] Kataria, H.R. and Patel, H.R. (2016) Radiation and Chemical Reaction Effects on MHD Casson Fluid Flow Past an Oscillating Vertical Plate Embedded in Porous Medium. *Alexandria Engineering Journal*, **55**, 583-595. https://doi.org/10.1016/j.aej.2016.01.019

[22] Lihonou, T.F., Monwanou, A.V., Miwadinou, C.H. and Orou, J.B.C. (2022) Active Control of the Instability of a Dynamic Laminar Boundary Layer on a Flat Impermeable Plate Subjected to a Magnetic Field. *Indian Journal of Physics*, **96**, 3591-3601. https://doi.org/10.1007/s12648-022-02284-5

[23] Shampine, L., Kierzenka, J. and Reichelt, M. (2000) Solving Boundary Value Problems for Ordinary Differential Equations in MATLAB with BVP4C. Tutorial Notes, 1-27.

[24] Biswas, R., Afikuzzaman, M., Mondal, M. and Ahmmed, S.F. (2018) MHD Free Convection and Heat Transfer Flow through a Vertical Porous Plate in the Presence of Chemical Reaction. *Frontiers in Heat and Mass Transfer*, **11**, 1-10. https://doi.org/10.5098/hmt.11.13

Nomenclature

B_0	Magnetic component (Wb·m^{-2})
C	Concentration of fluid (-)
$\tilde{C}$	Dimensionless fluid concentration (-)
C_f	Skin friction (-)
C_s	concentration susceptibility (J/kg·K)
C_p	Specific heat at constant pressure (J/m^3·K)
C_w	concentration at the plate surface (mol/l)
C_∞	concentration at far away from the plate (mol/l)
D_m	Molecular diffusivity of the concentration (-)
D_u	Dufour Number (-)
E	The electric field.
E_c	Eckert number (-)
F	The non-dimensional stream function
f or U	The mean velocity nondimensional profile.
f'	The first derivative of velocity.
f''	The second derivative of velocity.
F_w	Initial value of F
F_w^+	Initial positive value of F
F_w^-	Initial negative value of F
g	Acceleration due to gravity (m·s^{-2})
G_r	Grashof number (-)
G_m	Modified Grashof number (-)
J	The current density vector
k	Thermal conductivity (W/m·K)
k_1	Reaction rate constant (-)
k_p	Permeability of porous medium (-)
k^*	Darcy permeability (-)
k_T	Thermal diffusion ratio (-)
L	Plate length or maximum value of x
M	Magnetic parameter

N_u	Nusselt number (-)
P_r	Prandlt number (-)
Q	Heat absorption quantity (-)
S	Heat source parameter (-)
S_c	Schmidt number (-)
S_h	Sherwood number (-)
S_r	Soret number (-)
T	Temperature of fluid (K)
T_w	Temperature at the plate surface (K)
T_∞	Temperature at far away from the plate (K)
T_m	Mean fluid temperature (K)
$\tilde{T}$	Dimensionless fluid temperature (-)
U	Dimensionless primary velocity (m/s)
U_0	Uniform velocity (m/s)
V_0	Injection/suction velocity in the y direction
u , v	Velocity components (m/s)
U , V	Dimensionless velocity components
x , y	Dimensional cartesian coordinates (m)
X , Y	Dimensionless cartesian coordinates

Greek Symbols

β_T	Thermal expansion coefficient (-)
β_c	Concentration expansion coefficient (-)
ρ	Fluid density (kg·m^{-3})
∇	Nabla operator
$\phi = \overline{v}$	The amplitude function
δ or δ_{BL}	Boundary layer thickness
μ	Dynamic viscosity (Pa·s)
μ_e	The magnetic permeability
ν	Kinematic viscosity (m^2·s^{-1})
θ	The nondimensional coordinate

γ	Chemical reaction parameter (-)
ε_e	Absolute permittivity of the fluid
σ	The fluid electrical conductivity
$\uparrow$	Increase
$\downarrow$	Decrease